SLAC-PUB-5649
January 1992
(I)

PULSE-BY-PULSE ENERGY MEASUREMENT AT THE STANFORD LINEAR COLLIDER*

SLAC-PUB--5649

DE92 011520

G. Blaylock
University of California at Santa Cruz, CA 95064

D. Briggs, B. Collins, and M. Petree
Stanford Linear Accelerator Center, Stanford University, Stanford, CA 94309

Abstract

The Stanford Linear Collider (SLC) collides a beam of electrons and positrons at 92 GeV. It is the first colliding linac, and produces Z^0 particles for High-Energy Physics measurements. The energy of each beam must be measured to one part in 10^4 on every collision (120 Hz). An Energy Spectrometer in each beam line after collision produces two stripes of high-energy synchrotron radiation with critical energy of a few MeV. The distance between these two stripes at an imaging plane measures the beam energy. The Wire-Imaging Synchrotron Radiation Detector (WISRD) system comprises a novel detector, data acquisition electronics, readout and analysis. The detector comprises an array of wires for each synchrotron stripe. The electronics measure secondary emission charge on each wire of each array. A Macintosh II (using THINK C, THINK Class Library) and DSP coprocessor (using ANSI C) acquire and analyze the data, and display and report the results for SLC operation.

Presented at the Technical Conference and Expo, San Francisco, CA, January 15–17, 1992.

*Work supported by Department of Energy contract DE–AC03–76SF00515.

Introduction

The Wire-Imaging Synchrotron Radiation Detector (WISRD) system provides a pulse-by-pulse energy measurement at the Stanford Linear Collider [1] (SLC). The system measures the two beam energies using synchrotron radiation generated in Extraction Line Spectrometers (ELS). The synchrotron radiation falls on arrays of fine wires, and ejects electrons. Low-noise electronics digitizes the charge ejected from each wire. A Macintosh II and DSP accelerator acquire and analyze the data, calculate the energy and dispersion of both primary beams 120 times a second, and report the results.

An ELS in each beam line downstream of the Interaction Point (IP) provides a kinematic measure of beam energy. Each spectrometer produces two stripes of high-energy synchrotron radiation with critical energy of about 3 MeV. The angle between these stripes is inversely proportional to the beam energy. These two stripes of synchrotron radiation impinge on imaging planes, and the distance between the imaged stripes provides a measure of the beam energy.

The SLC Facility

Figure 1 shows a plan view of the SLC facility. It is the first colliding linac, and has produced Z^0 particles for High-Energy Physics measurements since April 1989. In operation, a small bunch of electrons collides with a small bunch of positrons at 120 Hz. Each bunch comprises a few times 10^{10} particles in a region measuring a few microns transverse and about a centimeter longitudinally, as they collide at the IP. The Linear Accelerator (Linac) is about two miles long, and accelerates the bunches of electrons and positrons to energies of about 45.5 GeV. The bunches emerge from the Linac and enter the SLC Arcs. A bending magnet separates the bunches. The electrons enter the North Arc and the positrons enter the South Arc. Near the IP, a set of superconducting quadrupole focusing magnets focuses both bunches to a few microns in the transverse dimensions, and they collide. After collision, pulsed magnets steer the bunches into the ELSs, with the electrons continuing to the South Dump, and the positrons to the North Dump.

The SLD detector [2] surrounds the IP. Z^0 particles produced in the collision decay at rest in the lab frame inside the SLD. Several detector

subsystems measure the momenta and energies of the decay particles and determine particle identities. On most beam crossings, the bunches merely pass through each other, but at some rate, a beam crossing includes an annihilation event, yielding a Z^0 particle. Physics analysis requires that the relative energy of each beam be measured to one part in 10^4 on every collision, at 120 Hz, and that the systematic error in the measured energy be less than 30 MeV.

The WISRD system data collection and control electronics are located near the SLD detector. The WISRD front end electronics and detectors are in the Arcs. The control of the SLC accelerator facility is in another building. The WISRD system reports beam energies and widths to SLC and SLD electronics locally. It also provides a graphical display to SLC operators remotely.

The Extraction Line Spectrometer

Figure 2 shows the electron ELS. There is another ELS for positrons. The beam of electrons enters from the left, proceeds through a hard-bend magnet that generates the initial synchrotron radiation stripe, through a reference magnet that provides the analyzing bend, then through a second hard-bend magnet that generates the final synchrotron radiation stripe. The bending angle through the reference magnet is proportional to the transverse field integrated along the length of the magnet, divided by the beam momentum. Both reference magnets and a spare were carefully surveyed before installation [3]. The magnetic fields of the reference magnets are monitored by flip coils that run the length of the magnet, and by NMR probes. Both measures of magnetic field are monitored through IEEE-488 electronics by another Macintosh II, located next to the WISRD system Mac. This second Mac informs the WISRD system Mac of the values of the reference bending fields through a CAMAC link.

The magnetic fields in the hard-bend magnets are high, yielding a critical energy of about 3 MeV for the synchrotron radiation produced. The reference magnet fields are much lower. They produce synchrotron radiation of lower intensity and lower critical energy, which is masked off. The bending planes of the hard-bend magnets are perpendicular to the bending plane of the

spectrometer magnet. Of the two imaged stripes per beam, one renders a narrow stripe and the other exhibits the energy dispersion of the beam.

The positions of the reference magnets and the positions of the wire arrays were carefully surveyed. The wires in each pair of arrays were surveyed at the 10 μm level before installation. The systematic errors of survey tolerances dominate the error in the energy measurement.

Secondary Emission Electron Production

The charge developed in each wire of the arrays depends on the intensity, energy spectrum, and angular dispersion of the synchrotron radiation produced in the hard-bend magnets. Figure 3 shows relative spectra of the synchrotron photons and ejected electrons. The top spectrum describes the photon production in the hard-bend magnets. These photons are produced in the vacuum of the beam pipe, but must traverse metal vacuum components and electronic shielding before they impinge on the WISRD wires. The attenuation in material gives rise to the filtered spectrum. Since the wires are of small diameter, they absorb only a small fraction of the incident synchrotron beam. The synchrotron photons interact mostly by the Compton process. The mean free path of Compton recoil electrons in the Copper of the wires is short at low energy, and for the most part, only those produced near the surface of the wire emerge. The total charge in one wire array scales with the integral of the ejected electron spectrum.

WISRD Detector

The WISRD detector is novel in its use of the Compton process for detecting synchrotron radiation [4]. The technique used previously involved phosphor screens for detection of synchrotron radiation. The principal advantage of the WISRD is its faster response. Figure 4(a) shows one WISRD detector. The major design challenge was mechanical stability and electrical resistivity, on a very small scale, in the presence of intense high-energy synchrotron radiation. Ninety-six Copper wires 75 μm in diameter, on 100 μm centers, are glued to a MACOR substrate. Electronic shielding and a vacuum canister surrounding each wire array are not shown. Figure 4(b) shows one wire array.

Electronics

Figure 5 shows a block diagram of the WISRD system. A Macintosh II computer provides the user interface and hosts Nubus peripherals. The National Instruments NB-DSP2300 DSP accelerator operates as a Nubus master to acquire and analyze the data. It uses MacVee Nubus and MacCC CAMAC modules as a Nubus-to-CAMAC interface [5]. The DSP calculates the charge on each wire of the four arrays. It then analyzes the distributions of charge and calculates the energies and widths of the two beams, on every event. The Macintosh II displays a sample of the full event stream. The display includes four histograms representing the charge on each wire of an array, after gain-offset corrections, with a report of the energy and width of both beams, and a histogram of the distribution of total energy in the last 10^5 events. In normal operation, the screen display is given over to the NTSC display converter, and the made available to a closed-circuit TV channel, observed in the Accelerator Control Room. Accelerator operators use this display as a convenient machine diagnostic tool. The DSP sends reports of the energies and widths of both beams through CAMAC to accelerator operations and detector operations on each event.

Figure 6(a) shows a block diagram of the front end electronics near the WISRD detector. In each Arc, an RF-enclosure houses electronics. Figure 6(b) shows a block diagram of the Data Acquisition Modules of Figure 6(a), with 24 channels per module. A LeCroy charge-sensitive preamplifier HQV-820 receives the wire signal. A shaping amplifier improves the signal-to-noise. A Calorimeter Data Unit (CDU) from Analytek serves as a Parallel-in/Serial-out analog memory. It samples each shaping amplifier output twice within a few microseconds—at the peak and valley of a bipolar pulse. An ADC digitizes the 48 sampled voltage levels and reports the values to a sequencer, which Manchester-encodes them. The encoded data are sent serially on long lines (≈600 feet for the North Arc, ≈1000 feet for the South Arc) to the CAMAC electronics of Figure 5. These long lines lie within a few feet of the beam lines for most of their length. Figure 7 shows the electronics in the CAMAC crate.

Software

The use of two distinct processors (Mac and DSP) for handling WISRD data attacks the two main requirements of the system: (1) a user-friendly interface for control and monitoring of the system; and (2) uninterrupted, high-speed processing of the data. The Mac performs run control (including downloading of code onto the DSP), error processing and display, file handling for calibration and survey constants, and periodic event display. Symantec's THINK C 4.0 provided the programming environment for the Macintosh. The object-oriented THINK Class Library furnished a starting point for the application shell, window and pane handling, menus, printing, and file management.

The NB-DSP2300 satisfies the second requirement for processing power. It runs in parallel with the Mac, asynchronously. It fetches the raw data and posts the computed results over Nubus and CAMAC, calculating the beam energies and widths from the wire charge distributions, and communicating periodically with the Mac for run control and error reporting. Software for this device is written in ANSI C, and compiled on the Mac using an optimizing cross-compiler/assembler/linker supplied by Texas Instruments for the TMS320C30 chip. The cross-compiler runs under MPW. Several features of the NB-DSP2300 have made it convenient for use as the primary computing and data acquisition engine. Its capability as a Nubus master is crucial in the data acquisition. Its ability to access Mac memory provides for asynchronous Mac/DSP communication. The optimizer requires at least a rudimentary knowledge of DSP assembly code, but provides the time-critical performance. Competition between the Mac and DSP for various shared resources is resolved transparently by Nubus protocol.

Figure 8 shows a distribution of completion times for typical events. The floating point performance improvement provided by the NB-DSP2300 is about a factor of 100 over a Macintosh II. Measured performance depends on the details of the application.

Performance

Figures 9(a) and 9(b) show that the pedestals (offsets) and the shape of the gain distributions as measured by calibration are stable. The measured energy

is only weakly dependent on channel-to-channel variations in gain and offset, due to the shapes of the measured distributions and the ratio of signal to noise. The typical noise, evaluated at the input of the preamplifier, amounts to about 1.5 femtoCoulombs. Background from beam pickup occurs on a few channels at a few times the noise. The error rate in the serial data transmission over the long cables in the beam environment is such that no errors in transmission have been detected that did not indicate a disconnected cable or equipment failure.

Figure 10 shows a typical event from the SLD engineering run of the summer of 1991. The dispersed stripes exhibit the energy distribution in the measured bunches. Slightly bimodal distributions are not uncommon, and vary on each event. The vertical axes for the four stripe histograms are in femtoCoulombs. At beam currents of $4*10^{10}$ particles per bunch, the charge on the central wires of the undispersed stripe often exceeds 200 fC per wire.

Clearing field electrodes close to the wire arrays are responsible for an effective baseline shift, proportional to total bunch charge. The effect is stronger near the edges, where the clearing field electrodes present more solid angle to the wires. Extensive diagnostic electronic measurements determined that the spatial structure of the baseline shift corresponds to electronic coupling of the wires to the clearing field electrodes. Measurements in operation show that the time structure of the analog wave form of the baseline shift is indistinguishable from that of the nominal wave form. In contrast, the time structure of beam pickup is the time-derivative of the nominal wave form.

Conclusions

The WISRD provides an energy measurement of each beam of the first linear collider, on a pulse-to-pulse basis at 120 Hz. The relative errors are less than one part in 10^4, and the systematic errors less than 30 MeV. The system has proved very reliable in operation. It provides a useful visual display of the energy dispersion for accelerator operations. Proper RF shielding and EMI measures suppressed the electronic background from the primary beams below levels of interest. Detector design requires more attention to image currents. The NB-DSP2300 DSP accelerator provides markedly improved

performance in Nubus data acquisition and computing power, and is crucial in this application. THINK C and the THINK Class Library provided a convenient path to a full-fledged Macintosh application for process control and display. The cross-compiler tools for the DSP provided an adequate programming environment.

Acknowledgments

The authors gratefully acknowledge J. J. Gomez y Cadenas of CERN; A. Hogan, J. Kent, M. King, W. Rowe, and S. Watson of University of California, Santa Cruz; M. Levi of Lawrence Berkeley Laboratory; F. Rouse of University of California, Davis; J. Tinsman of Radius Corp; C. Von Zanthier of KETEK GmbH, Haimhausen, Germany; and D. Wilkinson.

References

[1] "The Stanford Linear Collider," John R. Rees (SLAC), SLAC–PUB–5203, October 1989. 9 pp. Sci. Am. 261:No. 4:58, 1989

[2] "Overview of the SLD," Martin Breidenbach (SLAC), SLAC–PUB–3798, October 1985. 5 pp. Presented at Nuclear Science Symposium, San Francisco, CA, October 23–25, 1985. Nucl. Sci. Symp. 1985:46 (or see above page in IEEE Trans. NS–33, 1986).

[3] "Precision Measurements of the SLC Reference Magnets," S. Watson (UC, Santa Cruz), M. E. Levi (LBL, Berkeley), J. Nash (SLAC), SLAC–PUB–4908, March 1989. 3 pp. Presented at IEEE Particle Accelerator Conf., Chicago, IL, March 20–23, 1989.

[4] "Design of a Wire Imaging Synchrotron Radiation Detector," J. Kent, J. J. Gomez Cadenas, A. Hogan, M. King, W. Rowe, S. Watson, Christoph Von Zanthier (UC, Santa Cruz), D. Briggs (SLAC), M. E. Levi (LBL, Berkeley), SLAC–PUB–5110, January 1990. 5 pp. Presented at IEEE 1989 Nuclear Science Symposium, San Francisco, CA, January 15–19, 1990.

[5] These modules were developed at CERN. They are available in the USA through Sparrow and Associates, PO Box 6102, Mississippi State, MI.

Figure 1: Plan View of the SLC Facility
Plan view of the SLC facility, with SLD Detector and Extraction Line Spectrometers (ELS), not to scale. The WISRD CAMAC electronics and Macintosh II computer are about a hundred feet north of the SLD Detector.

Figure 2: The Extraction Line Spectrometer
Synchrotron radiation generated in the Horizontal Bend magnets falls on arrays of wires. Low-noise electronics measures the distributions of the charge ejected from each wire. The distance between the centroids of the two distributions measures the energy of the primary beam (electrons in this figure).

Figure 3: Particle Spectra
The graph shows the production spectrum of synchrotron radiation produced in the hard-bend magnets. It shows that part of the production spectrum incident on the wires, surviving attenuation in flight through metal components of the vacuum systems and RF shielding for the electronics. It shows the spectrum of recoil electrons in the wires, and the part of the recoil spectrum which results in electrons ejected from the wires. The lower three curves are rough analytic approximations. All curves are for 1010 particles in the primary beam. The total charge yield in one wire array scales with the integral of the ejected electron spectrum. These calculations are from J. Kent, UCSC.

Figure 4a: WISRD Detector Wire Array Pair
Two wire arrays are mounted together to intercept the two synchrotron radiation stripes. The RF shielding and vacuum canisters around the wires are not shown.

Figure 4b: One WISRD Wire Array
The target area is in a plenum flushed with dry Nitrogen. The bridge forms a seal. The 96 wires lie parallel in the target area, then fan out from the bridge and comb to individual pins at the four connectors.

Figure 5: WISRD System
A timing signal from the accelerator initiates data acquisition, and sends strobe signals to digitizing electronic modules in each arc. These report the charge on each wire of the four arrays to CAMAC modules. The NB-DSP2300 DSP Accelerator acts as a Nubus master. It uses the MacVee/MacCC pair to control the CAMAC crate. On each event at 120 Hz, it reads all the CAMAC raw data, performs gain-offset corrections per channel, calculates the energy

and width of each beam, and reports the energies and widths through CAMAC to the SLD detector and the SLC accelerator. The Macintosh II displays a sample of the events, including the charge distributions, after gain-offset corrections. The Macintosh monitor provides a view locally, and an NTSC converter provides the same view to accelerator operators. Another Macintosh II controls GPIB instruments and provides measurements of the magnetic fields in the reference magnets.

Figure 6a: Front End Electronics
In each arc, data acquisition modules provide low-noise digitized measures of the charge on each wire. The wires of the detector connect to the active electronics by well-shielded coaxial cables, about 20 feet long. Separate RF enclosures house the detector and the low-noise electronics.

Figure 6b: Data Acquisition Module Block Diagram
Each wire connects to a preamplifier and shaping amplifier, designed for low noise. The shaping amplifier provides a bipolar pulse. An analog memory (parallel-in/serial out) samples the positive- and negative-going peaks (a few microseconds apart) of all 24 channels. The Analog-to-Digital converter digitizes the 48 samples consecutively, to 12 bits of resolution. The sequencer controls the readout and conversion, and Manchester-encodes the serial data for transmission.

Figure 7: CAMAC Data Acquisition Electronics
Each 2-channel FIFO module receives the Manchester-encoded serial data from two data acquisition modules in an arc. It de-codes the streams and checks for transmission errors. Each Cable I/O module controls the data acquisition in one arc, including calibration levels. The Timing Generator controls the analog sampling, conversion, and transmission.

Figure 8: Distribution of Completion Times
The plot shows the relative frequency of completion times for the DSP accelerator. The NB-DSP2300 completes a data acquisition and analysis cycle well before the next beam-crossing occurs. The electronics permits data acquisition across CAMAC to the DSP during serial transmission, but the plot shows completion times for the case where the DSP waits until the end of serial data transmission before beginning CAMAC data acquisition.

Figure 9a: Autocorrelation Function of Electronic Gain
To measure the stability of calibration, all channels were calibrated many times over 60 hours. The autocorrelation function,

$$R_g(t) = \frac{\sum_{i=0}^{MaxWire} g_i(0) \cdot g_i(t)}{\sqrt{\left(\sum_{i=0}^{MaxWire} g_i^2(0)\right)\left(\sum_{i=0}^{MaxWire} g_i^2(t)\right)}}$$

where $g_i(t)$ is the gain of channel i measured at time t (in ADC counts/fC), exhibits a drift on the order of 3 parts in 10^6 in this time. The function measures the stability of the shape of the distribution of gains. The measured energy responds weakly to changes in gain that affect all channels proportionally.

Figure 9b: Pedestal Drift over Time
The plot shows the drift of the offsets or pedestals over time, using the same calibration results as in Figure 9a. Plotted is the function

$$\overline{\Delta P}(t) = \frac{\sqrt{\sum_{i=0}^{MaxWire} [p_i(t) - p_i(0)]^2}}{N_{wires}}$$

where $p_i(t)$ is the pedestal of channel i measured at time t. The graph is in femtoCoulombs. Typical noise of a channel is about 1.5 fC.

Figure 10: A Typical Event Display During the SLD Engineering Run
This typical event shows the charge distributions from the four wire arrays in femtoCoulombs, after gain-offset corrections. It also shows the calculated energies and widths of each beam, and the participation plots (logarithm of the frequency of measured energies of each beam, over the most recent 10^5 events. In this event, the positron bunch comprised about 4×10^{10} particles, and the electron bunch somewhat less.

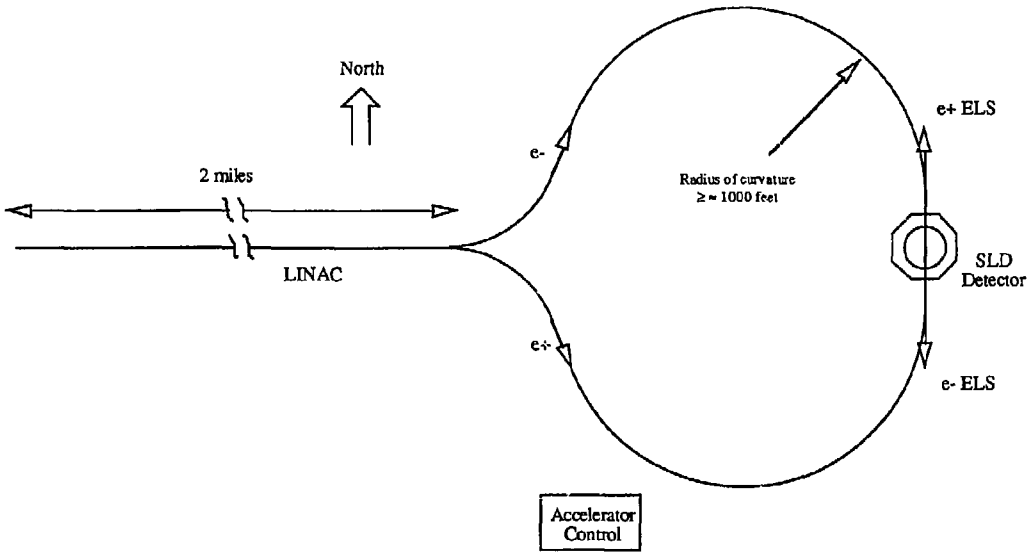

SLACPUB 5649
Pulse-by-Pulse Energy Measurement at the SLC
Fig. 1

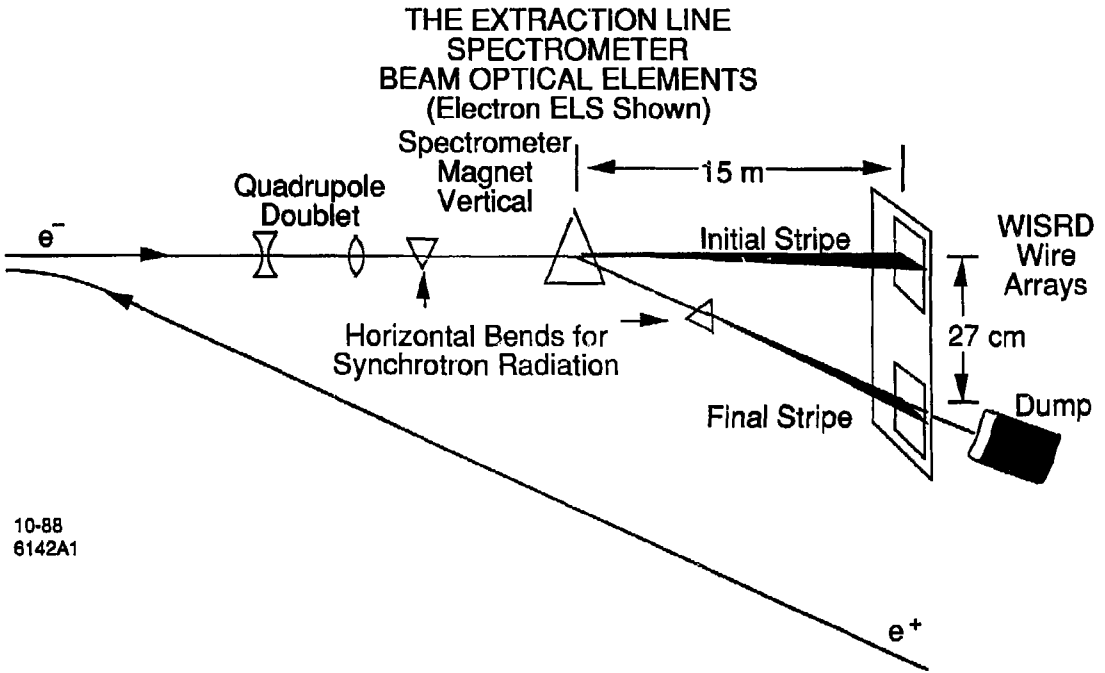

SLACPUB 5649
Pulse-by-Pulse Energy Measurement at the SLC
Fig. 2

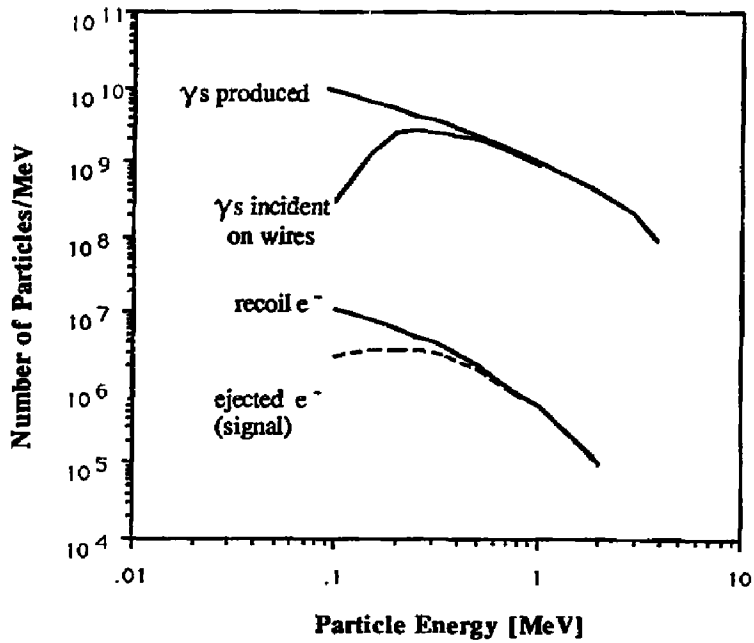

SLACPUB 5649
Pulse-by-Pulse Energy Measurement at the SLC
Fig. 3

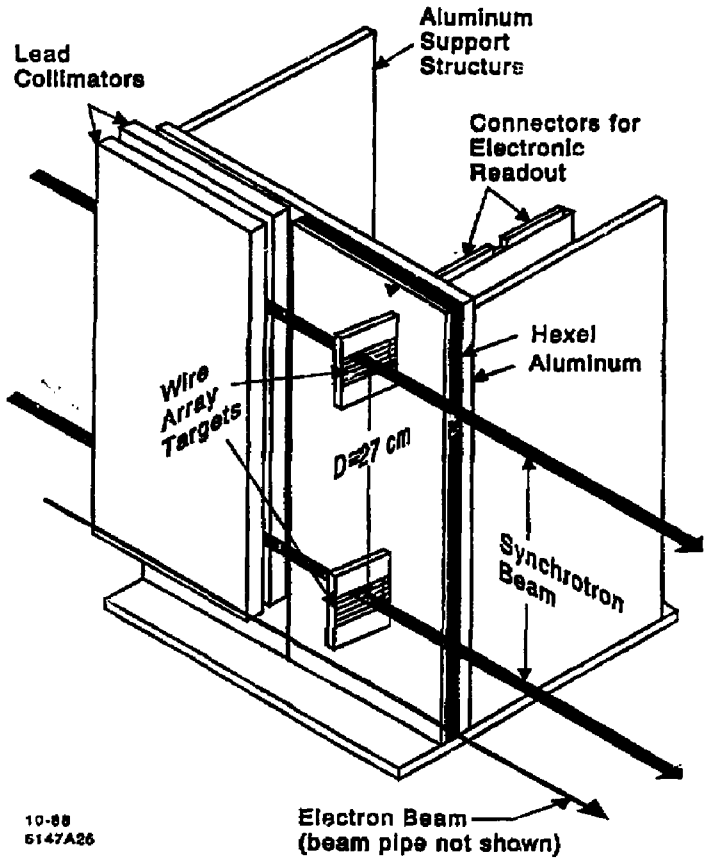

SLACPUB 5649
Pulse-by-Pulse Energy Measurement at the SLC
Fig. 4a

SLACPUB 5649
Pulse-by-Pulse Energy Measurement at the SLC
Fig. 4b

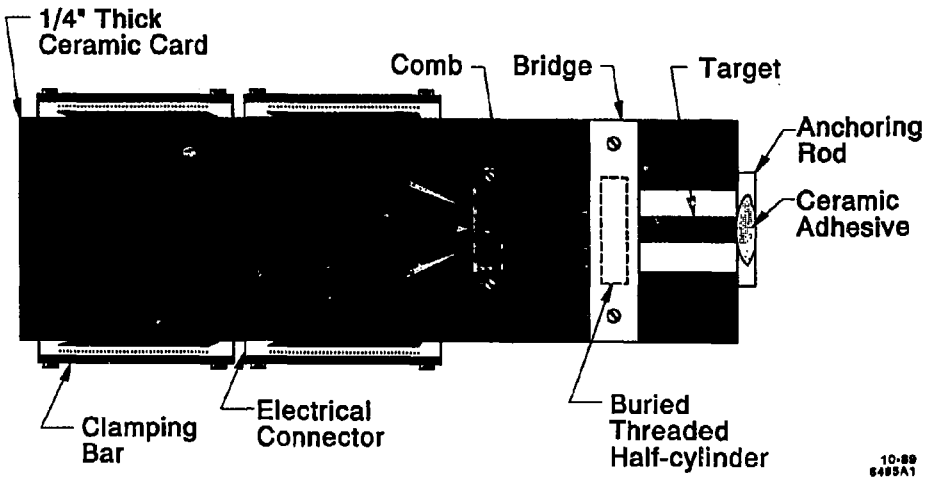

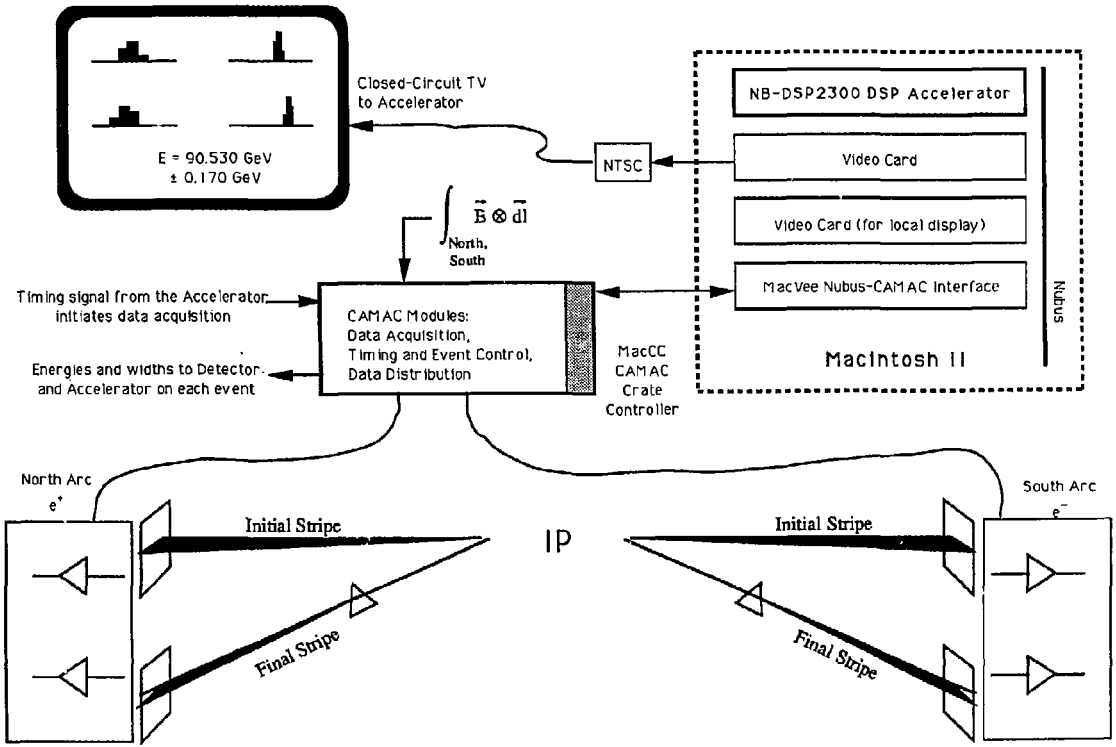

SLACPUB 5649
Pulse-by-Pulse Energy Measurement at the SLC
Fig. 5

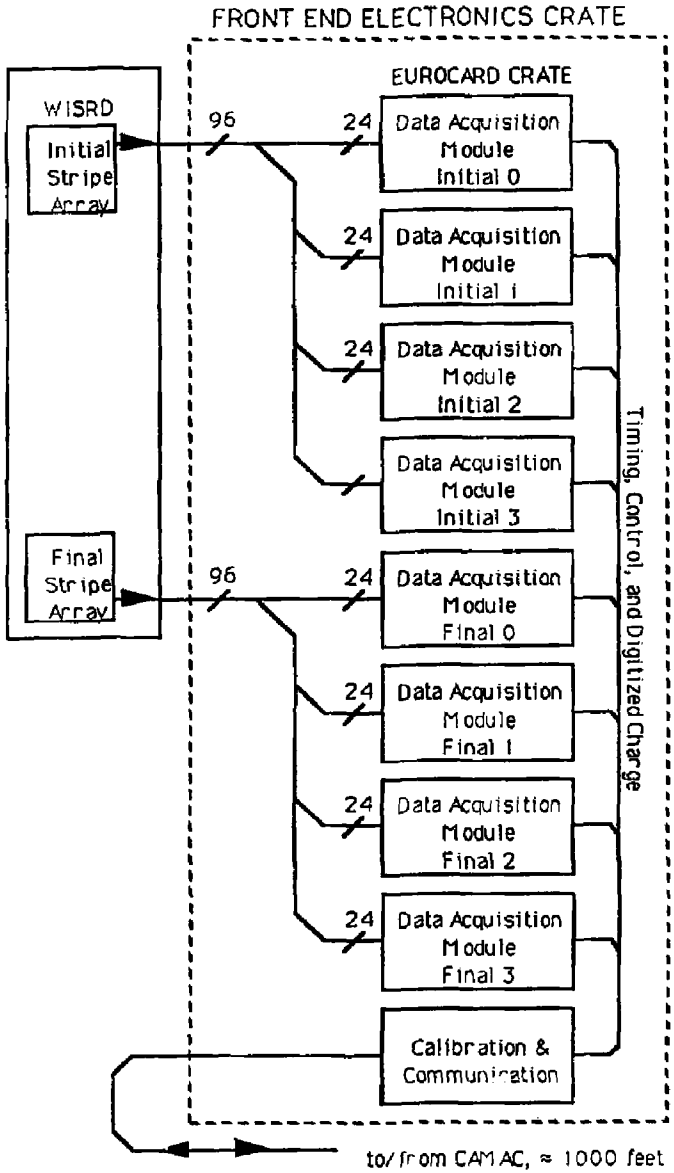

SLACPUB 5649
Pulse-by-Pulse Energy Measurement at the SLC
Fig. 6a

DATA ACQUISITION MODULE BLOCK DIAGRAM

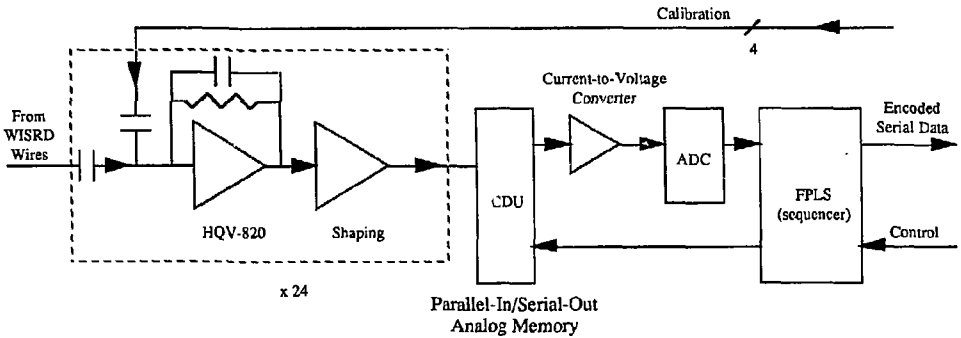

SLACPUB 5649
Pulse-by-Pulse Energy Measurement at the SLC
Fig. 6b

CAMAC ELECTRONICS

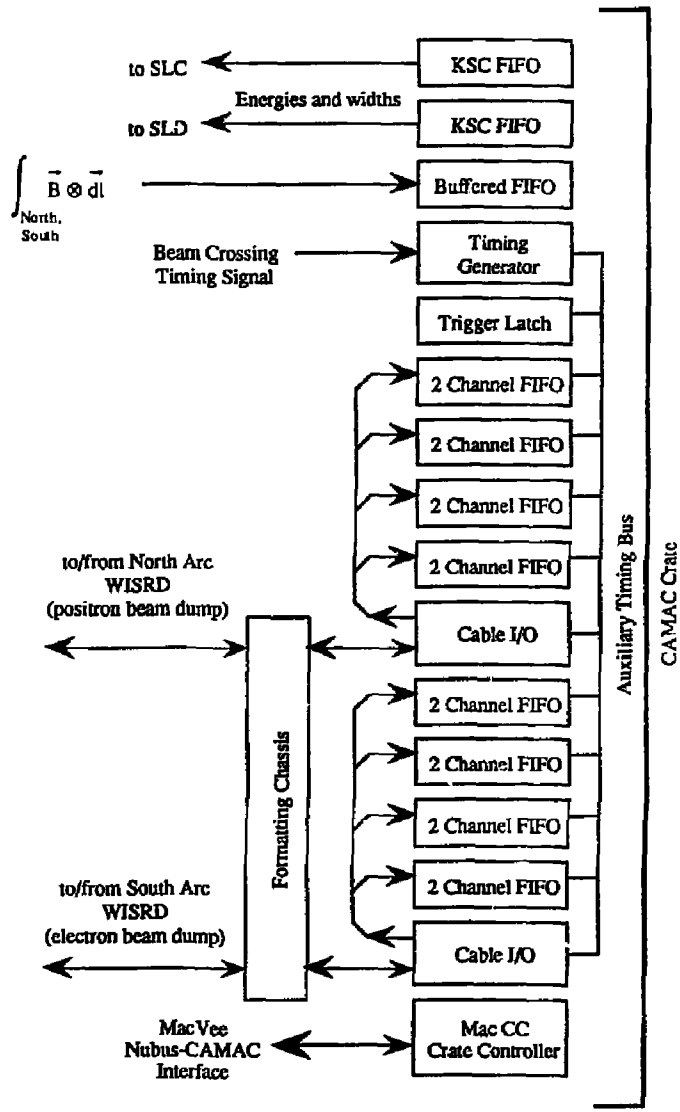

SLACPUB 5649
Pulse-by-Pulse Energy Measurement at the SLC
Fig. 7

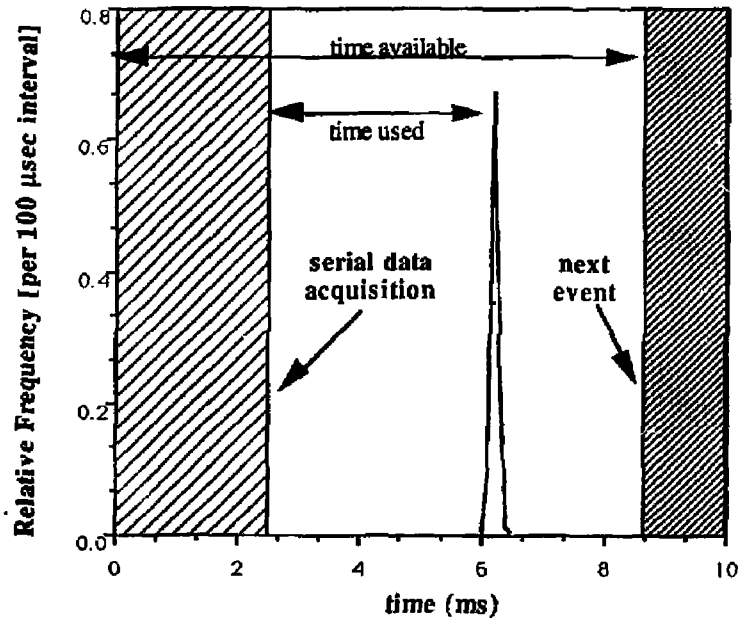

SLACPUB 5649
Pulse-by-Pulse Energy Measurement at the SLC
Fig. 8

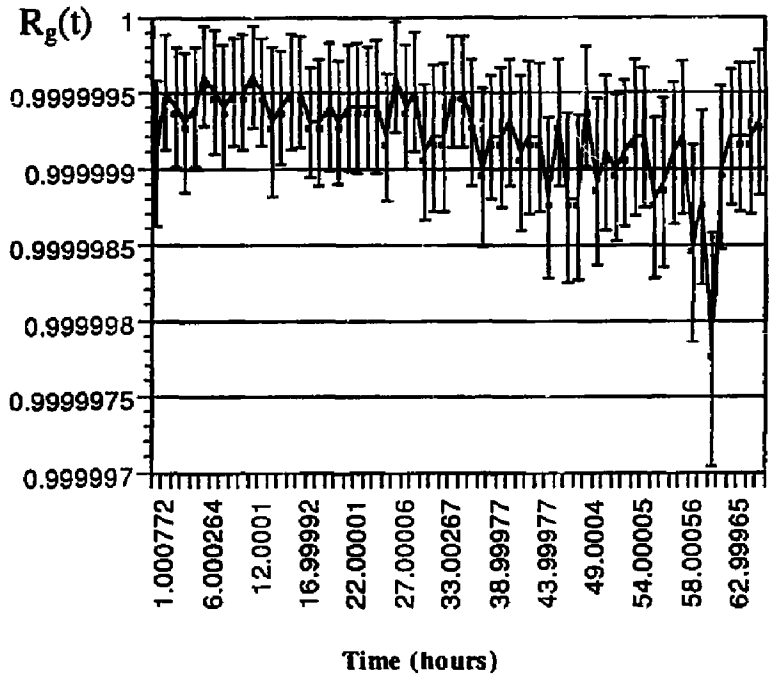

SLACPUB 5649
Pulse-by-Pulse Energy Measurement at the SLC
Fig. 9a

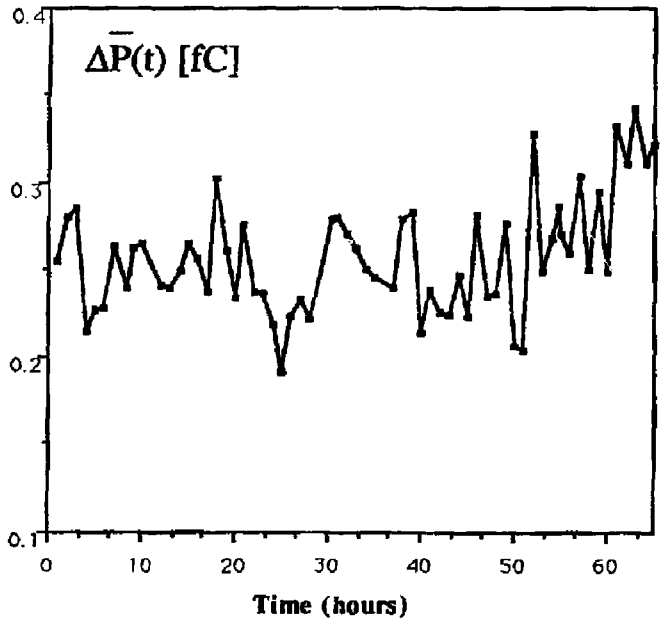

SLACPUB 5649
Pulse-by-Pulse Energy Measurement at the SLC
Fig. 9b

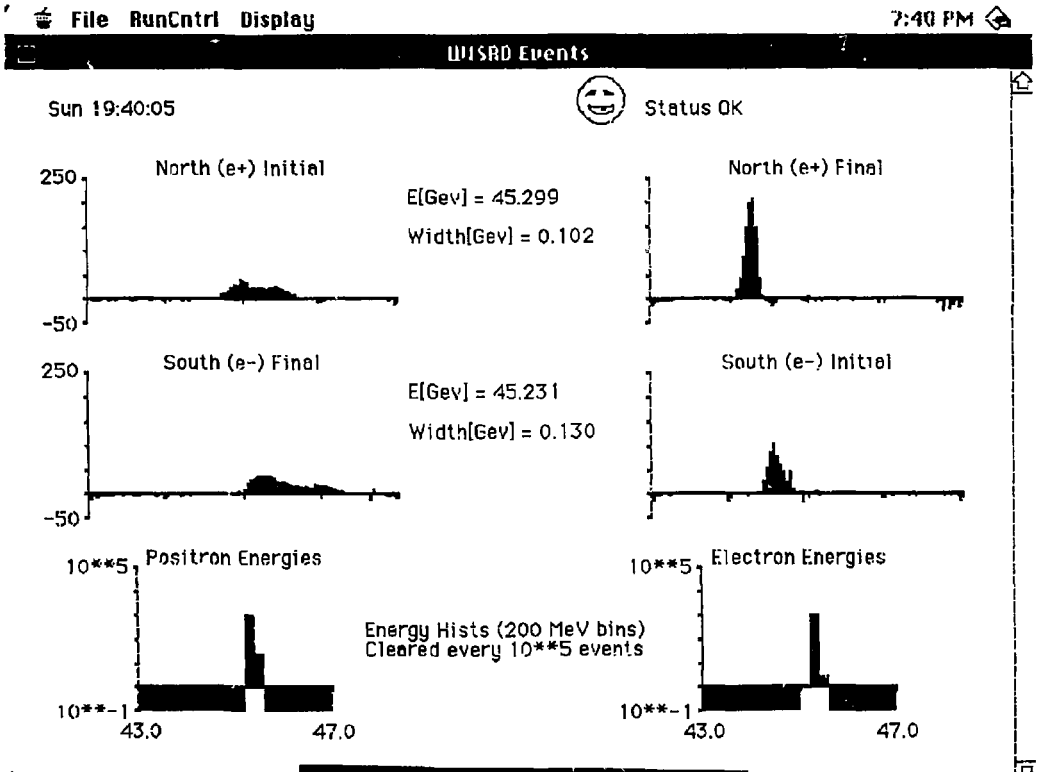

SLACPUB 5649
Pulse-by-Pulse Energy Measurement at the SLC
Fig. 10